Computational fluid dynamics simulation and optimisation of the threshing unit of buckwheat thresher for effective cleaning of the cleaning chamber

Saddam Hussain,[1] Decong Zheng,[1] Haiyan Song,[1] Muhammad Usman Farid,[2] Abdul Ghafoor,[3] Xinyi Ba,[1] Hao Wang,[1] Wenjun Wang,[1] Alam Sher,[4] Salah Jumaa Alshamali[5]

[1]College of Agricultural Engineering, Shanxi Agricultural University, Taigu, Shanxi Province, China; [2]Department of Structures and Environmental Engineering, University of Agriculture, Faisalabad, Punjab, Pakistan; [3]Department of Farm Machinery and Power, University of Agriculture, Faisalabad, Punjab, Pakistan; [4]Department of Agronomy, Ghazi University. D.G Khan, Punjab, Pakistan; [5]Deparment of Mechanical and Electrical Engineering, Albaath University, Homs, Syria

Abstract

Since a combined harvester's grain-cleaning method depends on the pneumatic separation of grain and chaff, the airflow's aerodynamic forces significantly affect cleaning efficiency. Based on buckwheat's theoretical and mechanical properties, a new threshing drum with cleaning key parts was developed to reduce the variability of cleaning efficiency of buckwheat community threshers caused by inefficient threshing and accumulation of residue within the threshing system. This cleaning arrangement includes two wind speed inlets, each composed of four thin pipes of the same length as the threshing drum. The computational fluid dynamics modelling approach simulated the threshing and cleaning performance at different wind velocities within the threshing unit. The results showed that when the two inlets work simultaneously and adopt different wind speeds, *i.e*., 12 m/s and 15 m/s, the wind speed is higher than the critical value of the floating rate buckwheat kernel. Under this condition, the wind speed inlet area was increased, and the flow field velocity between the threshing drum and the concave grid plate ranged from 3.8 m/s-8.3 m/s. The flow velocity below the plate ranged from 7 m/s-15 m/s, higher than the floating speed of buckwheat kernels, which was the best choice. Based on these simulation results, a centrifugal fan was designed, which meets the buckwheat thresher's cleaning performance.

Correspondence: Haiyan Song, College of Agricultural Engineering, Shanxi Agricultural University, Taigu 030800, Shanxi Province, China.
Tel.: +86.03546288400.
E-mail: haiyansong2003@163.com; 821867018@qq.com

Key words: Buckwheat thresher; clean system; computational fluid dynamics modelling; centrifugal fan; numerical simulation; threshing drum.

Acknowledgements: this work was supported by State Key Laboratory of Sustainable Dry land Agriculture (in preparation), Shanxi Agricultural University (No.202003-7); Major Special Projects for the Construction of China Modern Agricultural Industrial Technology System (No. CARS-07-D-2).

Received for publication: 13 July 2021
Accepted for publication: 21 December 2021.

©*Copyright: the Author(s), 2022*
Licensee PAGEPress, Italy
Journal of Agricultural Engineering 2022; LIII:1230
doi:10.4081/jae.2022.1230

This article is distributed under the terms of the Creative Commons Attribution Noncommercial License (by-nc 4.0) which permits any noncommercial use, distribution, and reproduction in any medium, provided the original author(s) and source are credited.

Introduction

In China, the demand for high-value crops like buckwheat is increasing day by day because of its high protein content and recognition as healthy food (Rodríguez *et al*., 2020). Various sized combine harvesters are used for mechanised harvesting of this crop. However, it has been observed that the existing machines are inappropriate for the small land-holding farmers in terms of harvesting performance, efficiency, and land conditions (Chen *et al*., 2018). China's buckwheat is mainly planted in hilly and mountainous areas. The planting area is scattered with narrow plots and complex terrain. Due to planting scale, geographical conditions, and economic factors, the mechanisation level of buckwheat is relatively backward, and the development is unbalanced.

To accommodate the various crops grown, combine harvesters use a range of threshing and separating units worldwide. In China, threshing and separating systems for buckwheat harvesting traditionally incorporate a transversely arranged threshing cylinder and a vertically arranged cylinder for further threshing and separation. A feeder conveyor, tangential flow threshing cylinder, vibrating, cleaning sieve, longitudinal axial flow threshing cylinder, transmission, engine, and crawler frame are standard components of such combines. The working method can be divided into cutting, harvesting, feeding, threshing, extracting the grain, and transferring the clean grain for temporary storage. Different oscillating sieves are used to separate the grains from the chaff and short stalks. Besides these sieves, the fan is a key component in the cleaning system because it develops the aerodynamic force necessary to separate impurities from grains (Liang *et al*., 2019). The harvesting process of cereals generally includes harvesting, baling, stacking, threshing, separation, and grain cleaning (Riaz *et al*., 2017). However, the buckwheat flowering period is long, the grain maturity is incredibly inconsistent, and the grain ripening time is as long as 30 to 60 days (Płażek *et al*., 2019). Therefore, choosing the right harvesting time and method is essential to ensure buckwheat's harvesting efficiency and harvest quality.

Various research has been done for the development and application work in buckwheat production machinery. Still, there are

Non-commercial use only

some problems in developing buckwheat harvesting equipment in China Lu and Deng (2017). For example, the development of buckwheat harvesting technology in China is relatively late. The system is imperfect, the threshing part effect is not satisfactory, and the impact of threshing and cleaning is not appropriate for the crop yield. A suitable threshing device and cleaning system are the keys to improve the buckwheat threshing efficiency. Therefore, the research on the threshing machine clean system has important practical significance. For buckwheat threshing and cleaning, the study and design of the machine suitable for threshing and cleaning operations are significant and prove beneficial to increase farmers' income and help adjust the agricultural structure of buckwheat in China (Huang *et al.*, 2018).

The use of computational fluid dynamics (CFD) for the computation and assessment of turbomachinery and fluid flow has imparted significant improvement in the design and development of large-scale systems without duplication of efforts needed for experimentations and re-designing. CFD modelling of fluid systems is based on the steady Reynolds-averaged Navier Stokes (NeS), leading to significant advances in various engineering applications (Ceyrowsky *et al*., 2018; Cravero and Marsano 2020). For example, centrifugal fans have the advantage of static pressure and high cleaning efficiency; thus, these are widely used in cleaning equipment (Cravero and Marsano, 2020). As fluid (usually air) is used in the cleaning systems for threshing machines, CFD can also be a helpful tool to check and analyse the cleaning efficiency of the threshing device's flow field. Although various research studies have been conducted for the enhancement of cleaning efficiency, most of the studies have primarily concentrated on optimizing the cleaning system's structural parameters by analysing airflow distribution inside the threshing unit. However, the pressure distribution and airflow velocity in different measuring points have not been analysed apart from an even airflow distribution.

Hence, based on the analysis of harvester's and thresher's research status, this study aims to design and simulate the threshing device with cleaning essential parts without considering the working load.

Materials and methods

The overall structure and working principle

The closed-cutting bar threshing device was implemented according to the buckwheat threshing and cleaning system requirements. The overall structure was mainly composed of: i) the drum; ii) the concave grid plate; iii) the draft wheel; and iv) the airflow cleaning system, which is shown in Figure 1A and B. Technical parameters of clean threshing device is listed in Table 1. The material entered the threshing device during operation through the inlet gap under the threshing drum's action. The closed threshing drum continuously impacted and smashed the material and removed buckwheat kernels. Those kernels fell onto the concave grid plate and passed through the grid concave. The plate fell then onto the shaker screen. As the exit gap became smaller, the buckwheat crop layer became thinner because the exit gap was much smaller than the inlet gap, so the buckwheat crop layer received the strongest rubbing force at the exit. At the exit gap, it was thrown away at a quarter of the threshing rate. When it was necessary to clean up the residual kernels, the fan was turned on, and the threshing device was cleaned through the designed wind speed inlet. In this design, a centrifugal fan was used in de-granulation.

Main technical parameters

The technical parameters of the clean threshing device are as follows.

Computational fluid dynamics modelling approach

The effluent's movement by the airflow is more complicated in the wind field of the threshing device. The flow field is observed at different inlets, different inlet wind speeds, and different inlet areas, and the motion laws such as velocity and pressure are analysed. The design and application of the cleaning system are of great significance. The main content is the numerical simulation of the threshing device's wind field using numerical simulation basic theory knowledge. The velocity cloud map and pressure cloud map are obtained.

The CFD program FLUENT 6.3 had been used to simulate the internal airflow structure of the CFF and the impact of different inlet flow speeds and inlet areas(Funaki *et al*., 2006). It has been shown that the two-dimensional CFD model can forecast fan output to a reasonable degree (Gebrehiwot *et al*., 2010). The Unsteady Reynolds-Averaged Navier Stokes (URANS) equations for transient, two-dimensional, viscous, incompressible fluids were solved. The rotation was modelled using the MRF method, which requires the division of the domain into a stationary area and a rotating area with an interface between the two. The turbulent flow was modelled using the standard k-ε model (Araya, 2019).

Computational domain, grid generation, and boundary conditions

In GAMBIT, an irregular pattern has been meshed. The method is to divide it into several small irregular patterns to mesh, accept GAMBIT's face for the Cooper meshing method, and start meshing. The meshed pattern is shown in Figure 2A, divided

Non-commercial use only

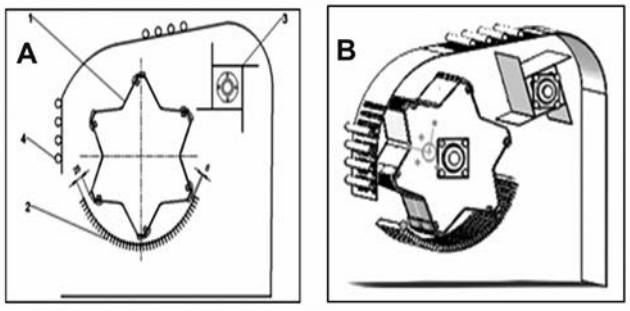

Figure 1. A) Overall structure of ribbon threshing device. B) Mechanical model of threshing device.

Table 1. Technical parameters of clean threshing device.

Element	Unit	Data
Diameter × length	mm	550×820
Roller speed	r/min	650~1500
Detachment rate	%	>94
Breakage rate	%	<3
Number of strokes	-	6
Bar model	-	D Type

into90,677 cells. The Y+ value of the mesh near the important regions (such as near the rotor walls) should be maintained between 30 and 100 when using the k-ε model to allow the use of wall functions to predict the behaviour of friction forces near the walls (ref ANSYS User's Guide). Also, mesh cells should not be skewed (the ideal value for skewness should be less than 0.9) to allow the CFD code to calculate all the field variables correctly.

In this design, because the rod's rotational speed from the roller and the draft wheel is a deviation, the airflow velocity around it is large, and the encrypted pattern is as shown in Figure 2B.

Selection of turbulence model

Turbulence is one of the important parameters while modelling the air flow in the closed structures. As a high speed jet is used for the cleaning of straws from the cleaning chamber of the thresher. Moreover, high speed rotation of the thresher drum and its counter air strike would cause a strong turbulence in the device Hence it is very important to study the turbulence within the thresher units. The turbulent numerical calculations include two methods: The Eulerian method and the Lagrangian method. It is impossible to have a model that can solve all problems in theory. Therefore, attention must be given to whether the fluid is compressible, the accuracy requirement, the special feasible problem, the finiteness of the computer, *etc*. Only after understanding these basic principles can one choose a suitable model.

k-ε model

The standard k-ε model is a semi-empirical model that uses model transport equations to calculate the turbulence kinetic energy (k) and dissipation rate (ε). The model transport equation for is derived from the exact equation, but the model transport equation was developed by physical reasoning and had no similarity to its mathematically precise counterpart (Menter, 1997).

The k-ε model was developed on the assumption that the flow is completely turbulent and that the effects of molecular viscosity are minimal. As a result, the conventional model is only valid for completely turbulent flows. The parameters values for standard k-ε model is listed in Table 2.

Its governing equations are:

$$\frac{\partial(\rho k)}{\partial t}+\frac{\partial(\rho k u_i)}{\partial x_i}=\frac{\partial}{\partial x_j}\left[\left(\mu+\frac{\mu_t}{\sigma_k}\right)\frac{\partial k}{\partial x_j}\right]+G_K+G_b-\rho\varepsilon-Y_m+S_k \quad (1)$$

$$\frac{\partial(\rho\varepsilon)}{\partial t}+\frac{\partial(\rho\varepsilon u_i)}{\partial x_i}=\frac{\partial}{\partial x_j}\left[\left(\mu+\frac{\mu_t}{\sigma_\varepsilon}\right)\frac{\partial\varepsilon}{\partial x_j}\right]+C_{1\varepsilon}\frac{\varepsilon}{k}(G_k+C_{3\varepsilon}G_b)+C_{2\varepsilon}\rho\frac{\varepsilon^2}{k}-S_\varepsilon \quad (2)$$

$$\varepsilon=\frac{\mu}{\rho}\left(\frac{\partial\mu_i}{\partial x_k}\right)\left(\frac{\partial\mu_i}{\partial x_k}\right) \quad (3)$$

$$G_k=\mu_i\left(\frac{\partial\mu_i}{\partial x_j}+\frac{\partial\mu_j}{\partial x_i}\right)\frac{\partial\mu_i}{\partial x_j} \quad (4)$$

$$G_b=\beta g_i\frac{\mu_i}{Pr_i}\frac{\partial T}{\partial X_i} \quad (5)$$

$$\beta=-\frac{1}{\rho}\frac{\partial T}{\partial x_i} \quad (6)$$

In the above equation, G_k represents turbulence kinetic energy generation due to mean velocity gradients, G_b represents turbulence kinetic energy generation due to buoyancy, Y_m represents the contribution of fluctuating dilatation in compressible turbulence to the overall dissipation rate, and C_{1e}, $C_{2\varepsilon}$, and C_3 are constants in these equations. s_k and s_ε are turbulent Prandtl numbers for k and εu respectively. User-defined source words are S_k and S_ε.

Renormalisation group k-ε model

It is like the standard k-ε model, with higher reliability and accuracy, and provides data analysis formulas for the turbulence model. Using a mathematical approach known as renormalisation group (RNG) techniques, the RNG-based k-ε turbulence model is constructed from the instantaneous Navier-Stokes equations. The analytical derivation gives a model with different constants than the conventional k-ε model, and extra variables and functions in the k and ε transport equations (Wang and Hu, 2012). The parameters values for standard RNG-based k-ε model is listed in Table 3.

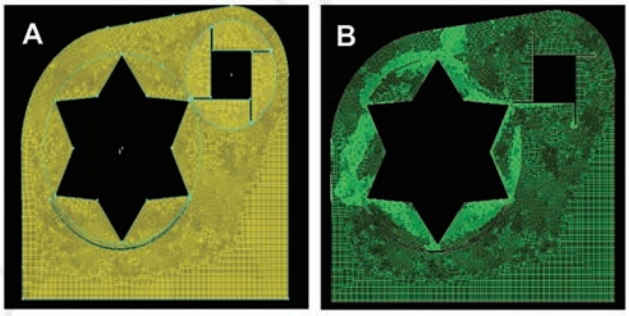

Figure 2. A) Threshing device grids. B) Adaptive encrypted grid.

Table 2. Standard k-ε model parameter values.

Parameter	Values
∂_k	1.0
σ_ε	1.3
Pr_t	0.85
$C_{1\varepsilon}$	1.44
$C_{2\varepsilon}$	1.92
$C_{3\varepsilon}$	0.09

Table 3. RNG k-ε model parameter values.

Parameter	Values
C_Z1	$1.42-\eta(1-\eta/\eta_0)/(1+\beta\eta_3)$
η_0	4.28
β	0.0015
η	Sk/ε
s	$\sqrt{(2s_{ij}\,s_{ij})}$
C_μ	0.085
C_{Z2}	1.68
σ_k	0.71
σ_z	0.79

Non-commercial use only

The model equation is:

$$\frac{\partial(\rho k)}{\partial t}+\frac{\partial(\rho U_j k)}{\partial x_j}=\frac{\partial}{\partial x_j}\left[\frac{\mu_{eff}}{\sigma_k}\frac{\partial k}{\partial_x}\right]+G_k-\rho\varepsilon \quad (7)$$

$$\frac{\partial\rho\varepsilon}{\partial t}+\frac{\partial(\rho U_j k)}{\partial x_j}=\frac{\partial}{\partial x_j}\left[\frac{\mu_{eff}}{\sigma_k}\frac{\partial_\varepsilon}{\partial_x}\right]+\frac{\varepsilon}{k}(C_{\varepsilon 1}G_k+C_{\varepsilon 2}\rho\varepsilon) \quad (8)$$

In the above equation, G_k represents turbulence kinetic energy generation due to mean velocity gradients, G_b represents turbulence kinetic energy generation due to buoyancy, Y_m represents the contribution of fluctuating dilatation in compressible turbulence to the overall dissipation rate, and $C_{1\varepsilon}$, C_2, and C_3 are constants in these equations. s_k and s_ε are turbulent Prandtl numbers for k and ε, respectively.

The k-ε model gives good results when the wall y+ is less than 1 without wall functions. It also performs well when y+ near the wall is between 30 and 100, but it requires wall functions. Fluent offers both options depending on grid resolution near walls.

Parameter setting of boundaries and initial conditions

Two wind speed inlets and exits are selected in the design, and different wind speeds, various wind speed inlets, and different inlet areas are used to simulate the wind field of the threshing device at the two wind speed inlets. The centrifugal fan is selected to clean the threshing device. The airflow cleaning is based on whether the airflow speed is higher than the buckwheat's floating speed. The cleaning can be performed when the airflow velocity is higher than the buckwheat's floating speed. The force diagram of the grain, as shown in Figure 3.

In Figure 3:

$$P = K\,\rho\,A\,v^2 \quad (9)$$

where: K: coefficient of drag (dimensionless); ρ: density (kg/m^3) A: reference section (m^2); v: velocity (m/s).

Critical velocity of the object:

$$V=\sqrt{\frac{mg}{KA\rho}} \quad (10)$$

where: m: mass (kg); g: acceleration of gravity (m/s^2); K: coefficient of drag; A: reference section (m^2); ρ: density (kg/m^3).

According to the critical speed of buckwheat and the mechanical design manual, the inlet wind speed sets to different wind speeds, various wind speed inlets, and inlet areas to simulate the wind flow distribution in threshing device.

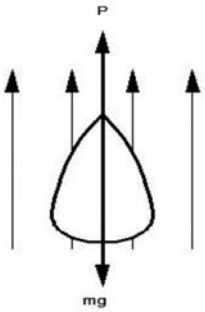

Figure 3. Grains stress diagram.

Results and discussion

Simulation results and analysis - Velocity distribution analysis

Case 1 (Analysis of the first inlet velocity flow field)

The above is the corresponding velocity cloud obtained at the first inlet velocity of the thresher at 12 m/s and 15 m/s, respectively. It can be seen from the Figure 4A and B that the wind speed is relatively low, the drum and the grid are concave.

The velocity of the flow field above the grid concave is 3.1 m/s-4.2 m/s, and the velocity of the flow field under the grid concave plate is 4.2 m/s-8.5 m/s. When the wind speed is relatively high, the speeds of both above and below the grid concave are 3.1 m/s-3.9 m/s and 5.5 m/s-12 m/s, which are both significantly lower than the floating speed of buckwheat grains. Therefore, this scheme is not advisable.

Case 2 (Analysis of the second inlet velocity flow field)

A speed inlet is provided at another location of the thresher. The first speed inlet is closed, and the flow field simulation of the threshing apparatus's wind field is determined under conditions where only the second speed inlet is open.

For the second wind speed inlet, when the wind speed is relatively low, the flow velocity between the threshing drum and the concave grid plate is 3.0 m/s-4.2 m/s, and the flow velocity below the grid concave plate is 3.0 m/s-5.4 m/s, when the wind speed is relatively large, the corresponding speed is 3.0 m/s-3.7 m/s ,which is still lower than the floating speed of buckwheat grains, which is not suitable. The velocity maps of the 2nd inlet wind speeds of 12 m/s and wind speed of 15 m/s are shown in Figure 4C and D.

Case 3 (Flow field simulation analysis of same wind speeds at two inlets)

When the two inlets are open simultaneously, the wind speed is relatively low. The flow velocity between the threshing drum and the concave grid plate is 3.2 m/s-4.5 m/s, and the flow velocity below the grid concave plate is 5.9 m/s-13m/s. When the wind speed is relatively large, the flow velocity between the threshing drum and the concave grid plate is 3.2 m/s-4.0 m/s, and the flow velocity below the grid concave plate is 6.4 m/s-16 m/s, which is lower than the floating speed of buckwheat kernels. This scheme is also not desirable. The velocity map for the two inlets adopt the same wind speed of 12 m/s and 15 m/s are shown in Figure 4E and F.

Case 4 (Flow field simulation analysis of different wind speeds at two inlets)

When the two wind speed inlets adopt different wind speeds, the clearing flow field's rate is similar. The flow field velocity between the threshing drum and the concave grid plate is 3.5 m/s-7.6 m/s. However, the flow velocity below the grid concave plate is 6.5 m/s-13.5 m/s, equal to the floating speed of buckwheat kernels, so this solution is still not desirable. The velocity map when the firs inlet wind speed is less than the second inlet wind speed and when the 2ndinlet wind speed is set to be smaller than the 1stinlet wind speed is shown in Figure 4G and I.

Case 5 (Flow field simulation analysis of different wind speeds at two inlets and different wind speed inlet areas)

The following method is adopted to change the wind speed inlet area's size, and the simulation analysis is continued for two

Non-commercial use only

wind speed inlets at different inlet wind speeds. In this state, adding a ventilation pipe, which increases the inlet area of 0.05 m^2, the analysis results are shown in Figure 5.

According to the graph analysis, the cleaning effect after increasing the wind speed inlet area is better. This is because the cleaning flow velocity between the threshing drum and the concave grid plate is 3.8 m/s-8.3 m/s, and the flow velocity below the grid concave plate is 7 m/s-15 m/s, which is higher than the floating speed of buckwheat kernels. Therefore, opening two wind speed inlets at different wind speeds is the best choice after increasing the wind speed inlet area. From all the above speed cloud maps, it is possible to analyse them.

During the threshing machine cleaning work, the wind speed gradually weakens from the inlet to the clearing area, and the actual air supply intensity is higher than that of the buckwheat grain. Selecting suitable air supply strength can ensure clean threshing and reduce cost. The air supply speed is not as large as possible. Too much wind speed is easy to take the buckwheat grain and waste, resulting in loss of output and increased power consumption. Therefore, the design increases the wind speed inlet area and opens two inlets simultaneously. A wind speed inlet and different wind speeds are designed to achieve the best cleaning results.

Pressure distribution analysis

The threshing device's wind field will have a specific pressure drop during the airflow cleaning due to the energy loss Tang Li (2018). Generally, these pressures will reduce the bar threshing device's working efficiency, but the threshing device's work can be improved in a certain sense. The cause of energy loss may be due to the rotation of the gas stream in the threshing device, or the energy loss caused by the friction of the gas stream in the air inlet and the air intake device's inner wall.

At different inlets and inlet wind speeds, the pressure of the wind field of the threshing device is different. The following is the pressure cloud map obtained under different conditions, and the pressure distribution of the wind field of the threshing device can be observed.

Case 1 (Analysis of the pressure at the first inlet)

The flow field simulation of the pressure-wind field with different wind speeds at the first wind speed inlet is analysed. The corresponding pressure cloud map obtained at first velocity inlet of the thresher at different inlet wind speeds of 12 m/s and 15 m/s, respectively, as shown in the Figure 5A and B. Because the velocity distribution is unequal, the pressure distribution is also uneven.

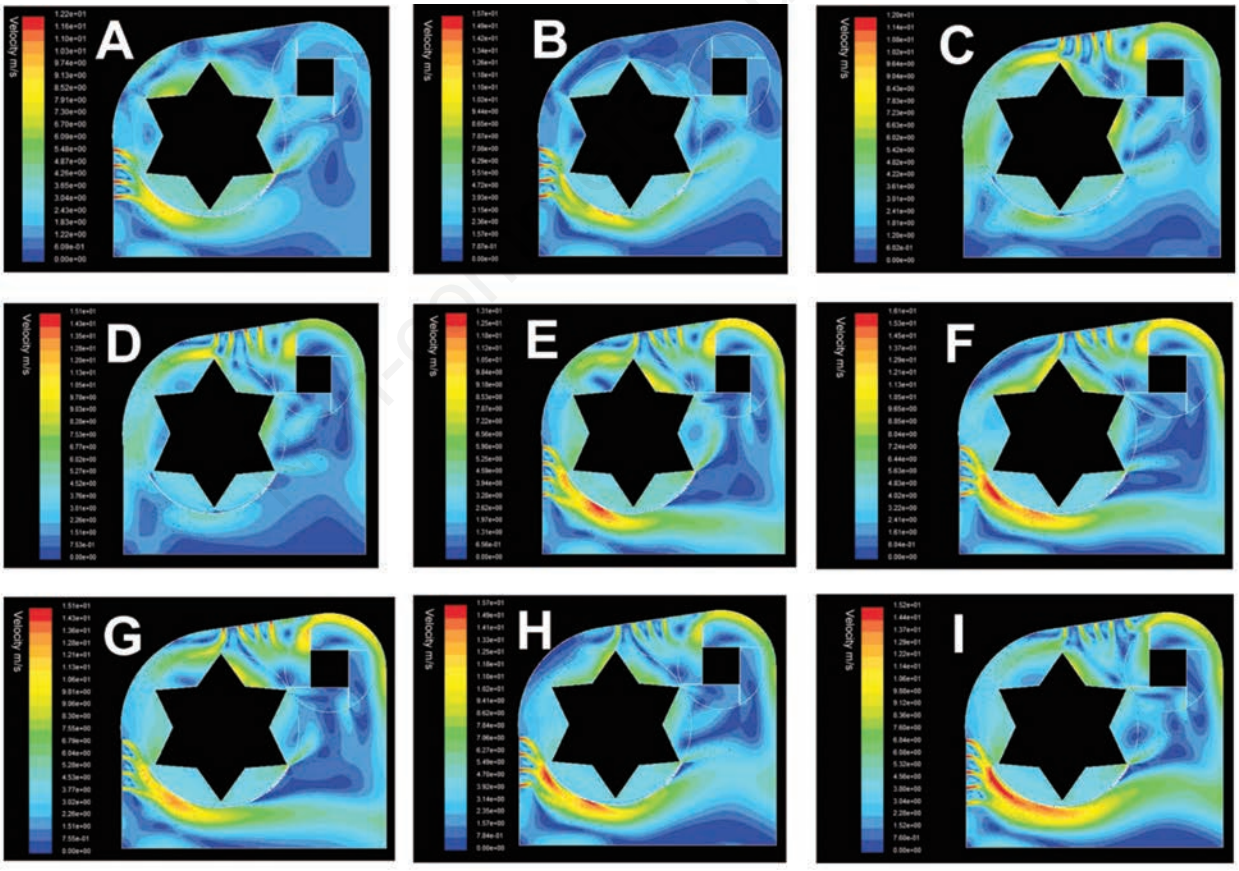

Figure 4. A) The velocity maps of the 1st inlet wind speeds of 12 m/s. B) The velocity map of the 1st inlet wind speed of 15 m/s. C) The velocity maps of the 2nd inlet wind speeds of 12 m/s. D) The velocity map of 2nd inlet wind speed of 15 m/s. E) When the two inlets adopt the same wind speed of 12 m/s. F) When the two inlets adopt the same wind speed of 15 m/s. G) When the first inlet wind speed is less than the second inlet wind speed. H) When the 2nd inlet wind speed is set to be smaller than the 1st inlet wind speed. I) Clouds of different wind velocity at two entrances after increasing entrance area.

The pressure in the surrounding space of the threshing drum, the drafting wheel to the affluent, and the waste discharge port is gradually lowered.

Case 2 (Analysis of the pressure distribution of the second inlet)

A speed inlet is provided at another location of the thresher. The first speed inlet is closed, and the flow field simulation of the threshing apparatus's wind pressure is determined under conditions where only the second speed inlet is open.

The corresponding pressure cloud map obtained at the second velocity inlet of the thresher at different inlet wind speeds of 12 m/s and 15 m/s, respectively, as shown in the Figure 5C and D. The velocity distribution is uneven, resulting in uneven pressure distribution. The pressure from the threshing drum's surrounding space, the drafting wheel to the affluent, and the waste discharge port are gradually reduced. The threshing is performed when the first wind speed inlet is operated. The pressure of the wind farm of the device is large, and when the inlet of the wind speed is changed to second inlet, the wind internal pressure condition of the threshing device changes.

The pressure cloud diagram for the second inlet wind speed of 12 m/s and 15 m/s is shown in Figure 5E and F.

Case 3 (Analysis of pressure distribution between two inlets at the same wind speed)

The flow field simulation of the pressure-wind field with wind speeds at two wind speed inlet is analysed. The pressure cloud is represented in Figure 5G and H under the conditions of opening two wind speed inlets at the same wind speeds.

Case 4 (Analysis of pressure distribution at different wind speeds of two inlets)

The flow field simulation of the pressure-wind field with different wind speeds at the first wind speed inlet is analysed. Then, the flow field simulation of the pressure-wind field with varying wind rates at the second wind speed inlet is analysed, and the pressure flow field simulation of the same wind speed at the two wind speed inlets is analysed.

Under the conditions of opening two wind speed inlets at different wind speeds, the pressure cloud after increasing the inlet area is shown in Figure 5I.

It can be obtained from the analysis of Figure 5 that when the first wind speed inlet is opened, the pressure between the threshing drum and the concave grid plate is higher than the pressure value below the concave plate. When the second inlet of the wind speeds opened, the pressure value between the threshing drum and the

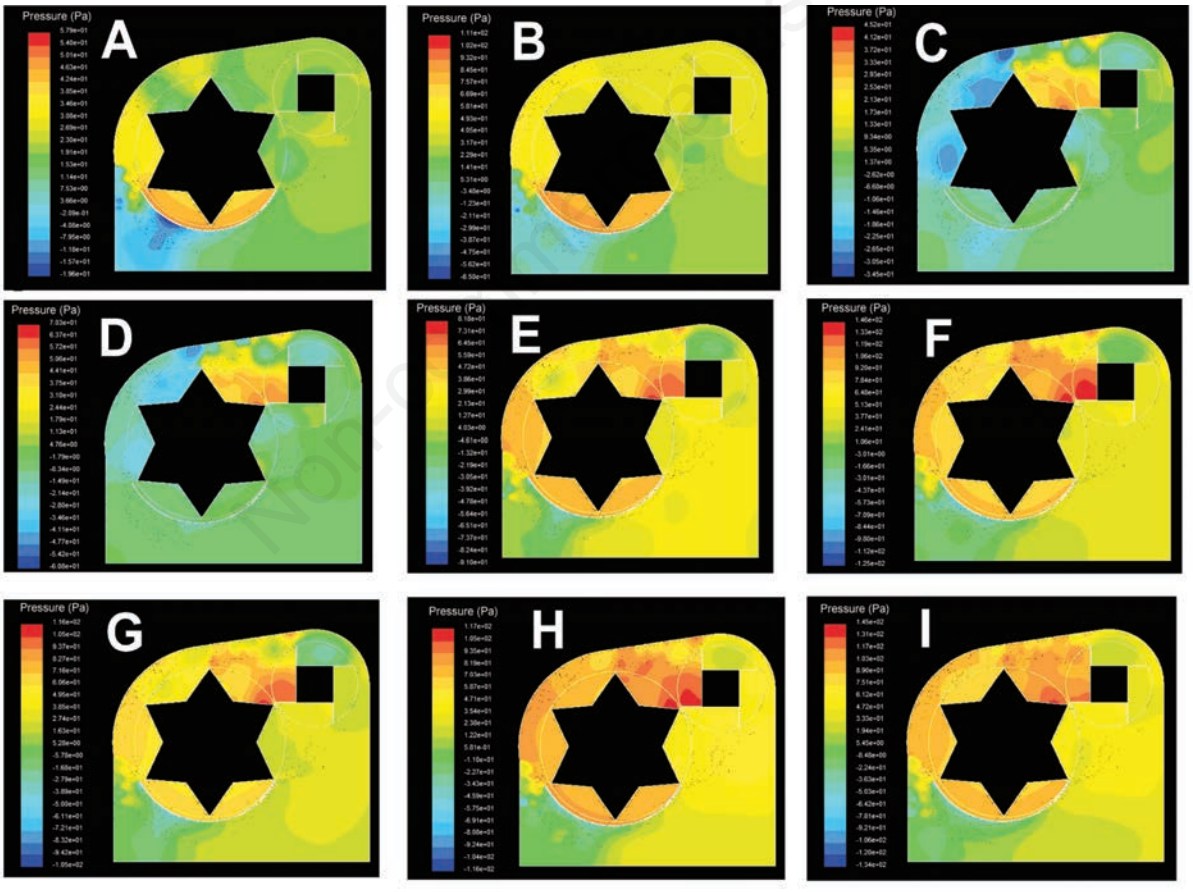

Figure 5. A) The pressure cloud diagram for the 1st inlet wind speed of 12 m/s. B) The pressure cloud diagram for the 1st inlet wind speed of 15 m/s. C) The pressure cloud diagram for the 2nd inlet wind speed of 12 m/s. D) The pressure cloud diagram for the 2nd inlet wind. E) The pressure cloud diagram with different wind speeds at the 1st wind speed inlet. F) The pressure cloud diagram with different wind speeds at the 2nd wind speed inlet. G) The pressure cloud diagram when both inlets are open at the wind speed of 12 m/s. H) The pressure cloud diagram when both inlets are open at the wind speed of 15 m/s. I) Pressure contours of two inlets with different wind speeds after increasing the inlet area.

concave grid plate is substantially the same as the pressure value under the concave plate, which is not conducive to cleaning the residual grain on the grid concave plate. So, the scheme of opening only the second wind speed inlet is not advisable. The pressure value around the threshing drum and the drafting wheel is greater than the remaining part's pressure value. The distribution of this pressure value is beneficial to the buckwheat's threshing and cleaning of the residual grain. The pressure of the threshing and cleaning part can be analysed from the above pressure cloud map distribution.

Model validation

According to the simulation result, the best air inlet speed ranges from 7 m/s to 15 m/s. In the actual experiment, the fan is working at 2800 rpm with an area of each outlet 0.05 m^2 having air velocity approximately 14 m/s, which is appropriate for grain cleaning. Experiments on the buckwheat threshing machine are carried out on a test bench to analyse the distribution of the threshing outputs and confirm the simulations' dependability (see Figure 6).When working, the buckwheat is placed on the conveyor belt and fed through the bridge to enter the inner and outer drum rotary threshing device. The extracted mixture falls into the cleaning box. Under the action of the reciprocating cleaning sieve and the cleaning fan, the grain and debris are cleaned. Optionally, the grains are output by the grain auger, and the sundries and straw are discharged from the grass discharge port. A blowing pipe is arranged inside the threshing device, and the pipe is evenly opened with blowing ports. The compressed air generated by the fan enters the blowing pipe through the windpipe and is blown out from the blowing port to blow off the materials remaining in the threshing device to achieve the clean threshing device effect. During the threshing process, the fan is turned on all the way, and every time the threshing is completed, the thresher needs to be cleaned three times, each time about 40 seconds. The quality of the residual grains obtained in the test data is the quality of the residual grains obtained after the three cleanings are completed. The single factor test was used to obtain the optimal conditions of the feed rate, the rotation speed of the inner drum, and the rotation speed of the outer drum. The design-Expert software Box-Behnken central combination design method was used for the experimental design, and the test results in Table 4 were obtained.

Figure 6. Internal and external drum rotary threshing device.

Table 4. The single factor test result for the optimal conditions of the feed rate, the rotation speed.

Orthogonal test										
Serial number	Feeding amount (kg/s)	Rotation speed of inner drum (r/min)	Outer drum speed (r/min)	Kernel quality	Threshing loss quality	Residual kernel quality	Broken kernel quality	Loss rate %	Residual rate %	Fragmentation rate %
1	0.5	450	0	1855.57	5.87	1.45	0.11	0.32%	0.08%	0.01%
2	0.5	500	50	1755.19	5.13	1.08	0.21	0.29%	0.06%	0.01%
3	0.5	500	–50	1525.63	5.84	0.91	0.88	0.38%	0.06%	0.06%
4	0.5	550	0	1665.32	4.89	0.85	0.04	0.29%	0.05%	0.00%
5	0.6	450	50	1470.48	4.18	1.10	0.08	0.28%	0.07%	0.01%
6	0.6	450	–50	1575.13	4.65	1.19	0.52	0.29%	0.08%	0.03%
7	0.6	500	0	1690.07	3.83	1.04	0.18	0.23%	0.06%	0.01%
8	0.6	500	0	1548.96	1.72	0.89	0.19	0.11%	0.06%	0.01%
9	0.6	500	0	1790.48	1.90	1.24	0.24	0.11%	0.07%	0.01%
10	0.6	500	0	1170.35	2.16	0.73	0.28	0.18%	0.06%	0.02%
11	0.6	500	0	1635.47	3.20	0.99	0.13	0.20%	0.06%	0.01%
12	0.6	550	50	1660.55	4.93	0.95	0.82	0.30%	0.06%	0.05%
13	0.6	550	–50	1585.67	3.64	0.99	0.27	0.23%	0.06%	0.02%
14	0.7	450	0	1855.53	4.90	1.72	0.02	0.26%	0.09%	0.00%
15	0.7	500	50	1370.51	4.37	0.86	0.40	0.32%	0.06%	0.03%
16	0.7	500	–50	1755.39	2.37	1.14	0.63	0.13%	0.07%	0.04%
17	0.7	550	0	1935.11	6.38	1.48	0.26	0.33%	0.08%	0.01%

Non-commercial use only

Conclusions and prospects

Based on buckwheat's material and mechanical properties, this paper designed a closed cut-flow bar threshing device with a length of 820 mm and a diameter of 550 mm, which solved the high cutting rate of buckwheat head and closed granules to prevent entanglement. This threshing device is equipped with a centrifugal fan, and the power required by the fan is calculated according to each parameter of the centrifugal fan. The fan is connected to a pipe with a diameter of 100 mm. At the two wind speed inlets, four thin pipes with the same length of 820 mm and a diameter of 27 mm are provided in the same direction as the bar threshing drum. A circular hole with a diameter of 12 mm and a spacing of 6 mm is provided above the road for the de-granulation cleaning system. The GAMBIT software is used to pre-process the wind field of the threshing device. The motion ANSYS (FLUENT) software performs numerical simulation and flows field analysis on the threshing device's wind field. Using velocity and distribution analysis, it is concluded that the inlet area, the flow field velocity between the threshing drum and the concave grid plate is 3.8 m/s-8.3 m/s, and the flow field velocity below the grid concave plate is 7 m/s-15 m/s, which is larger than the floating of buckwheat grains is the best choice for cleaning system.

Due to practical constraints, only the confirmatory tests for flow field simulation analysis of different wind speeds at two inlets and various wind speed inlet areas are performed, and the simulated and experimental data are compared. The front-end cleaning load was high, but the overall distribution was better than in the other two cases where the external roller rotated in three directions because the grains, chaff, leaves, and petals were concentrated in the front of the threshing roller and the short straws were distributed in the back.

References

Araya G. 2019. Turbulence model assessment incompressible flows around complex geometries with unstructured grids. Fluids. 4:81.

Ceyrowsky T., Hildebrandt A., Schwarze R. 2018. Numerical investigation of the circumferential pressure distortion induced by a centrifugal compressor's external volute. ASME Turbo Expo 2018: Turbomachinery Technical Conference and Exposition, American Society of Mechanical Engineers Digital Collection.

Chen Q.F., Huang X.Y., Li H.Y., Yang L.J., Cui Y.S. 2018. Recent progress in perennial buckwheat development. Sustainability. 10:536.

Cravero C., Marsano D. 2020. Criteria for the stability limit prediction of high speed centrifugal compressors with vaneless diffuser: part I - flow structure analysis. ASME Turbo Expo 2018: Turbomachinery Technical Conference and Exposition, American Society of Mechanical Engineers Digital Collection.

Funaki J., Kimata N., Hisada M., Hirata K. 2006. Aspect-ratio and Reynolds-number effects on short-span cross-flow impellers without casings. JSME Int. J. Series B. Fluid Thermal Eng. 49:1197-205.

Gebrehiwot M.G., Baerdemaeker J.D., Baelmans M. 2010. Numerical and experimental study of a cross-flow fan for combine cleaning shoes. Bioproc. Biosyst. Eng. 106:448-57.

Liang Z., Li Y., Xu L. 2019. Grain sieve loss fuzzy control system in rice combine harvesters. Appl. Sci. 9:114.

Menter F.R. 1997. Eddy viscosity transport equations and their relation to the k-ε model. J. F. Eng. 119:876-84.

Płażek A., Słomka A., Kopeć P., Dziurka M., Hornyák M., Sychta K., Pastuszak J., Dubert F. 2019. Effects of high temperature on embryological development and hormone profile in flowers and leaves of common buckwheat (Fagopyrum esculentum Moench). Int. J. Mol. Sci. 20:1705.

Riaz M. 2017. Harvesting, threshing, processing, and products of rice. In: Chauhan, B.S., Jabran, K., Mahajan, G. (Eds.), 2017. Rice production worldwide. Springer International Publishing AG, Switzerland, pp. 419-53.

Rodríguez J.P., Rahman H., Thushar S., Singh R.K. 2020. Healthy and resilient cereals and pseudo-cereals for marginal agriculture: molecular advances for improving nutrient bioavailability. Front. Genet. 11. [Epub ahead of print].

Tang L., Zheng Y., Changang D. 2018. Numerical simulation of internal flow field of cyclone dust collector based on fluent. Coal Technol. 37:270.

Wang J.Y., Hu X.J. 2012. Application of RNG k-ε turbulence model on numerical simulation in vehicle external flow field. Appl. Mech. Mater. 170-173:3324-8.

Xiaona H., Weilong D., Kunkun Z., Songke F., Zhijie L., Fuzeng Y. 2018. Research status and development trend of buckwheat harvesting machinery. Agri. Mach. 2018:84-90.

Non-commercial use only